Available online at www.sciencedirect.com
ScienceDirect
Journal of the European Ceramic Society 31 (2011) 85–95
www.elsevier.com/locate/jeurceramsoc

An indentation model for erosive wear in Al_2O_3/SiC nanocomposites

I.P. Shapiro [a,*], R.I. Todd [b], J.M. Titchmarsh [b], S.G. Roberts [b]

[a] University of Manchester, Materials Science Centre, Grosvenor Street, Manchester M1 7HS, UK
[b] University of Oxford, Department of Materials, Parks Road, Oxford OX1 3PH, UK

Received 29 April 2010; received in revised form 1 July 2010; accepted 20 July 2010
Available online 15 September 2010

Abstract

The erosive wear resistance of Al_2O_3 has been shown to be improved by the addition of 5 vol.% of sub-micron sized SiC particles to form a 'nanocomposite', in agreement with previous results. The erosive wear was measured directly, and also estimated by an indentation model consisting of closely spaced grids of indentations that mimic the effect of successive particle impacts; in the model, particle impacts cause sub-surface cracking but loss of material from the surface occurs only from an impact within a region damaged by a previous impact. The volume of material lost from within indentation grids was used to predict the wear rate. These predictions agreed well with the directly measured values.

The commonly observed change in fracture mode from intergranular for Al_2O_3 to transgranular for nanocomposites was confirmed. Transgranular fracture can allow a smaller volume of material to be removed during an impact and hence increase erosion resistance.

Keywords: B. Nanocomposites; C. Fracture; C. Wear resistance; D. Al_2O_3; D. SiC

1. Introduction

1.1. Nanocomposites

'Nanocomposites', consisting of Al_2O_3 with a few percent of sub-micron sized SiC particle additions, initially caused great excitement as they were reported to show considerable increases in strength[1] and increased toughness[2] compared to Al_2O_3. Subsequent work has not been able to reproduce these results.[3,4] However, it is well-established that the fracture mode changes from characteristically intergranular for Al_2O_3 to transgranular when SiC is added.[5,6] The wear resistance of nanocomposites has also been consistently found to be greater than that of alumina during abrasion[7,8] and erosion.[3,9,10] Nanocomposites also exhibit smoother surfaces compared to Al_2O_3 after identical polishing treatments.[11]

1.2. Wear testing

Erosion of Al_2O_3 results in two regimes: 'mild' and 'severe' wear.[12] Mild wear is thought to proceed through plastic deformation whereas severe wear involves brittle fracture. Miranda-Martinez et al.[13] found that, for the erosion conditions they used, smaller grain size (1 μm) Al_2O_3 wore in the 'mild' regime (smooth wear surface) and larger grain size (12 μm) Al_2O_3 wore in the 'severe' regime (rough wear surface). A related effect is that the wear rate of Al_2O_3 has a strong dependence on grain size.[13,14] Even for a given grain size, Al_2O_3–SiC nanocomposites are found to have lower erosive wear rates than Al_2O_3.[3,9,10] (Al_2O_3–SiC nanocomposites also generally have finer grain sizes than monolithic alumina, further increasing their wear resistance.) Kumar et al.[15] also measured a further reduction in abrasive wear rate when 1 wt.% Y_2O_3 sintering aid was added to 5 vol.% SiC nanocomposites. However, absolute values of wear rate cannot confidently be compared between the various different studies as they used different wear conditions and equipment.

Reduced abrasive wear rates are also observed for nanocomposites compared to Al_2O_3. For example, Ortiz-Merino and Todd[8] found the wear rate with 5 vol.% SiC was less than half that of Al_2O_3 of similar grain size when abraded with 45 μm

* Corresponding author.
E-mail address: ian.shapiro@manchester.ac.uk (I.P. Shapiro).

0955-2219/$ – see front matter © 2010 Elsevier Ltd. All rights reserved.
doi:10.1016/j.jeurceramsoc.2010.07.038

diamond. Similarly pin on disk wear testing under aggressive conditions has shown a marked reduction in wear rate for SiC nanocomposites compared to Al_2O_3.[16,17]

Ortiz-Merino and Todd[8] attributed the improvement in abrasive wear resistance of the nanocomposites to the change in fracture mode (from intergranular to transgranular) and developed a model where the wear rate is dependent on the area fraction of 'grain pullout'. The amount of grain pullout tends to be reduced in the nanocomposites as transgranular fracture allows a volume smaller than the whole grain to be pulled out rather than the whole grain as would occur in Al_2O_3. This hypothesis directly links the changes in wear rate to the change in fracture mode. Kara and Roberts[10] observed a greater degree of transgranular fracture on the eroded surfaces of nanocomposites and so the mechanism described by Ortiz-Merino and Todd may also apply to erosive wear. Recent work[7] has shown that a secondary factor in the improvements in wear resistance in the nanocomposites is that intragranular SiC particles suppress the formation of microcracks during plastic deformation by indentation or abrasion.

1.3. Modelling erosion behaviour

The way materials are damaged by erosion was linked to their indentation fracture behaviour by Evans and Wilshaw.[18] They found that lateral indentation crack extension could be enhanced by an adjacent indent and that, at a critical load and material dependent spacing, lateral cracks from each indent merge, and chips of material are lost from the surface. This process could provide a mechanism for erosive wear.

The extent of cracking around an indentation is linked to the material's toughness and hardness[19] and to the contact load; Evans and Wilshaw[18] developed an equation relating the wear rate to these parameters. However, for Al_2O_3–SiC 'nanocomposite' materials the SiC addition is found to significantly improve the wear resistance above that of Al_2O_3 despite having little or no effect on the hardness and toughness.[20]

Franco and Roberts[21] observed that in the early stages of erosive wear, isolated particle impacts produced sub-surface cracks but did not remove material in the form of wear debris. They hypothesised that a subsequent impact close to these cracks was what caused large amounts of debris to be released from the surface. Franco and Roberts[22] extended the theory that the interaction between two impacts controls wear to develop a quantitative model (Eq. (1)). This equation is based on the idea that an area of sample, A_0, is exposed to a flux of particles, Φ, each impact of which causes sub-surface cracking that 'primes' an area, a_p. A subsequent impact in the primed area will result in that area losing a flake of material with area a_w. At the start of erosion the total area of primed surface, A_p, will increase. However, as the removal of material restores fresh 'unprimed' surface the proportion of primed surface will reach a steady state, i.e. the rate of change in A_p with time, t, is zero:

$$\frac{dA_p}{dt} = (A_0 - A_p)\cdot\Phi\cdot a_p - A_p\cdot\Phi\cdot a_w = 0 \quad (1)$$

Hence:

$$\frac{A_p}{A_0} = \frac{a_p}{a_w + a_p} \quad (2)$$

The rate at which material is eroded is given by the number of impacts on the primed area ($A_p\cdot\Phi$) multiplied by the volume of material lost due to each of these impacts. The volume of material removed at each impact is related to its area (a_w), depth (d) and shape (α).

$$\frac{dV}{dt} = A_p\cdot\Phi\cdot a_w\cdot\alpha\cdot d = A_0\frac{a_p}{a_p + a_w}\Phi\cdot a_w\cdot\alpha\cdot d \quad (3)$$

The erosive wear rate is then the loss in material volume with respect to time per unit area:

$$R = \frac{a_p\cdot a_w\cdot\alpha\cdot d}{a_p + a_w}\Phi \quad (4)$$

Franco and Roberts[23] and Twigg et al.[24] suggested that the critical spacing between impacts (which is related to a_p) and the volume of material removed per impact in the primed area, a_w, can be estimated using arrays of indentations. Indentation arrays in alumina were made at loads equivalent to those of the impacting erodent particles with incrementally decreasing spacing to find the spacing at which material is lost from the surface due to lateral cracks linking up.[23,24] For an evenly distributed flux of erosive particles the smaller this critical distance, the longer the time between an area being primed and a particle impacting within the critical distance, and hence material being lost, leading to a lower erosive wear rate. Consequently the larger the critical distance the more frequently material is expected to be lost and the greater the erosive wear rate.

1.4. Outline of experiments

This work compares the erosive wear resistance of Al_2O_3 with an Al_2O_3–5 vol.% SiC nanocomposite material and also the effect of a Y_2O_3 sintering aid. The erosive wear resistance is compared to the damage that occurs within grids of indentations at various spacings. Quantification of the damage that occurs within these grids is used to test the validity of the erosive wear model of Franco and Roberts.[22]

2. Experimental methods

2.1. Materials preparation

Al_2O_3 and Al_2O_3–5 vol.% SiC 'nanocomposite' materials were produced using conventional processing with and without 0.15 wt.% Y_2O_3 sintering aid.[15] Appropriate quantities of Al_2O_3 (99.99% pure, AKP50, Sumitomo, Japan), SiC (>97.4% pure, 0.45 μm, UF25, H.C. Stark, Germany) and $Y(NO_3)_3\cdot 6H_2O$ (99.9% pure, BDH, UK; which decomposes to Y_2O_3 on heating) were ball milled in aqueous suspension for 3 h using Al_2O_3 media. To help dispersion 0.1 wt.% of Dispex A40 (Ciba, Switzerland) was added and, to help green body formation, 4 wt.% polyethylene glycol (PEG) was added. Pow-

Table 1
Sintering temperature, sintered density and grain size of the materials studied (from ref.[25]).

Material	Sintering temperature (°C)	Density (% theoretical)	Grain size (μm)
Al_2O_3	1550	99.7	3.17
$Al_2O_3 + Y_2O_3$	1550	100.0	2.25
$Al_2O_3 + SiC$	1775	99.2	1.91
$Al_2O_3 + SiC + Y_2O_3$	1750	100.1	2.03

ders were subsequently freeze-dried and uniaxially pressed at 137 MPa.

All materials were sintered in a flowing N_2 atmosphere (44 cm^2 cross-section alumina tube with a flow rate of 300 cm^3/min; LTF18, Lenton Furnaces, UK). The furnace was heated at 3 °C/min and held at the sintering temperature for 120 min before cooling at the same rate. The microstructure of these materials and the grain boundary segregation found to occur in them has been previously reported in detail.[25] The sintering temperatures, the sintered densities and grain sizes are summarised in Table 1. Before wear and indentation testing the sintered disks (~20 mm diameter) were flat-bed ground on each side and subsequently diamond polished with successive grades down to 1 μm.

2.2. Erosive wear testing

Erosive wear rate was measured using a 'rotating-jet slurry wear tester' designed, constructed and calibrated by Franco and Roberts[14] and illustrated in Fig. 1. The sample to be tested was held in the 'jet body' which was rotated at 180 rev/min in slurry consisting of 8 l of water and 1.5 kg of SiC grit particles with mean diameter ~780 μm (24C6, Washington Mills, Electro Mineral Ltd., UK).[14] The nylon jet body consisted of a funnel which accelerated the slurry into a tube at the end of which the sample was positioned. This ensured that particle impacts were normal to and confined to a particular area of the sample surface.

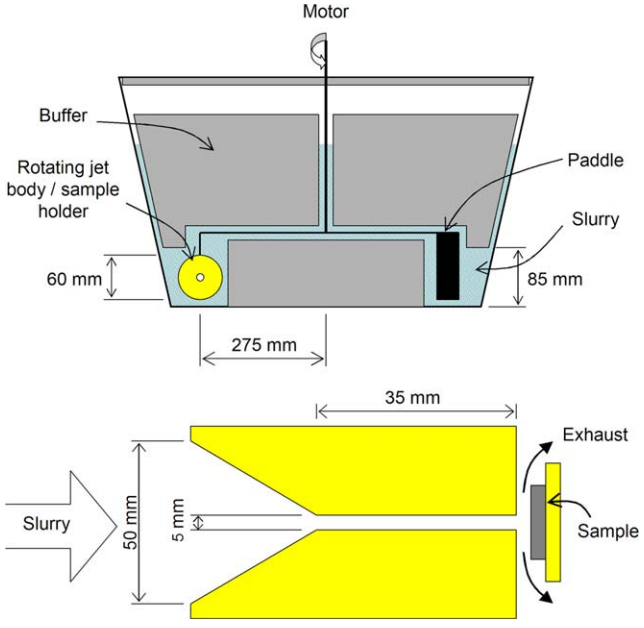

Fig. 1. Top: cross-section through the 'rotating-jet slurry wear tester'. Bottom: cross-section through the 'rotating-jet body'/sample holder.

Samples were initially weighed then eroded for a total of 12 h with the sample removed, dried and weighed after 1, 2, 4, 8 and 12 h erosion. The erosive wear rates were calculated using Eq. (5), where ρ is the specimen density, A_{imp} is the impacted area and $\Delta w/\Delta t$ the rate of weight loss. A_{imp} was calculated from the diameter of each of the wear craters (between 7.2 and 7.7 mm) and $\Delta w/\Delta t$ is taken as the gradient of the best fit line of weight loss against time.

$$R = \frac{1}{\rho \cdot A_{imp}} \left(\frac{\Delta w}{\Delta t} \right) \quad (5)$$

2.3. Fracture behaviour

The surfaces of samples eroded for 12 h were examined by SEM (S520, Hitachi, Japan). The degree of transgranular and intergranular fracture was estimated for each material. Micrographs were each divided up into a 10 × 10 grid and the number of rectangles which were considered to contain an area majority of intergranular fracture were counted; this figure was then used as the percent intergranular fracture. Areas on the surface (rather than points) were used due to the difficulty in assigning a fracture mode at a single point. However, statistical rigour would require that 100 defined points rather than areas should be sampled, although the differences in values are expected to be minor. Fracture was also induced by a crude 3-point bending rig using a G-clamp to load rectangular beams approximately 25 mm × 5 mm × 5 mm. The degree of transgranular and intergranular fracture on these surfaces was also estimated as above.

2.4. Erosive wear model

The impact of particles on the surface which occurs during erosive wear was modelled by arrays of indentations.

Indentations were made using a Berkovich indenter in an instrumented microhardness tester (CSM instruments, Switzerland). Sets of 9 indentations were made in square arrays with the central indentation made last. Arrays were made with indentation spacing of 40.0, 34.6, 30.0, 26.0, 22.5 and 19.6 μm with 100 μm gaps between grids repeated 3 times for each material.

The indentation load was set as 4.9 N. This load was an appropriate load for damage to interact at a suitable spacing to be observed in an optical microscope and is of the same order as the load (2 N) that Franco and Roberts[14] estimate as equivalent to the impact force of erosive particles under the conditions used in this work. Loading and unloading took 30 s with a 15 s hold period at maximum load.

An optical profilometer (white light interferometer, MicroXAM, ADE Phase Shift, USA) was used to measure the volume of material lost due to fracture within and around each set of 9 indentations. The instrument averaged the data from 5 focal scans to produce a height map. The software (MapVue version 6.32, ADE Phase Shift, USA) was used to calculate the

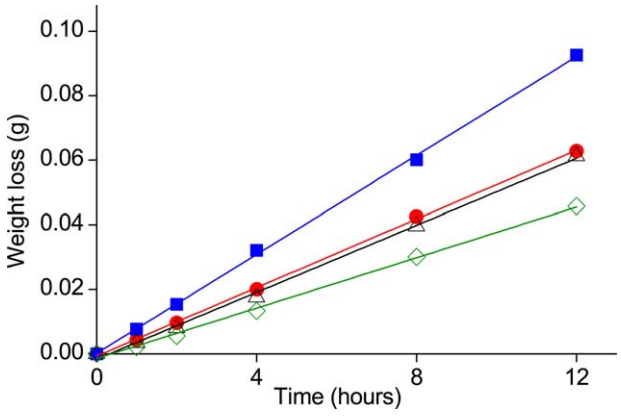

Fig. 2. Weight loss with time for four Al_2O_3 samples with no additions showing linear weight loss with time but variation between samples. Error bars lie within symbols.

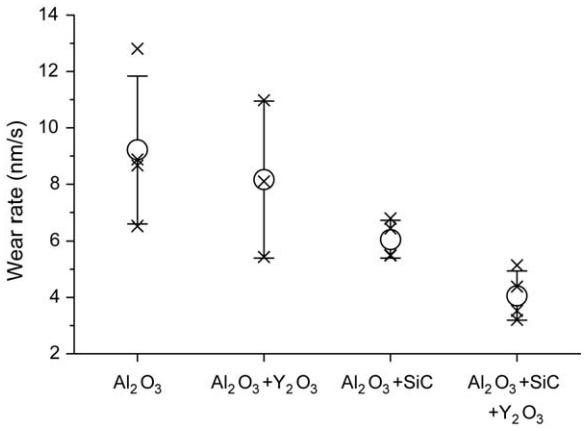

Fig. 3. Measured (×) and average values (◯) of erosive wear rate with standard deviation shown.

volume below the plane of the undisturbed surface outside the indentation grid. This volume represents the volume of material lost from the surface due to fracture plus the volume of the 9 indentations. The volume of material lost was averaged for the 3 grids at each spacing.

2.5. Sub-surface crack observation

Focused Ion-Beam milling (FIB 200, FEI Company, USA) was used to examine regions below the surface of apparently undamaged areas between indentations.

Samples were carbon coated to prevent charging and a 5 nA gallium ion beam was rastered over a 10 μm × 60 μm rectangle for 32 min. The beam raster was set to dwell longer at the top so as to make a stepped trench. Once this trench was completed the beam current was reduced to 1 nA and the beam rastered over a 60 μm × 1.5 μm rectangle positioned to overlap the top edge of the previous trench. This second pass cleaned and polished the surface of interest.

After etching the sample was removed, recoated with carbon and examined by SEM (JEOL 840F, Japan). The specimen was tilted 60° towards the detector resulting in the surface of interest being tilted 30° away from the detector. Samples were then thermally etched at 1475 °C for 30 min in a vacuum furnace (Lenton, $<10^{-8}$ mbar, 5 °C/min heating/cooling rate) to reveal the grain boundaries, then carbon coated and re-examined by SEM.

3. Results

3.1. Erosive wear

The weight loss was plotted against erosion time and found in all cases to give a straight line as shown for Al_2O_3 in Fig. 2. Due to variation in wear rate between specimens, at least 3 separate specimens of each material type were tested. The results of each wear test and the average for each material are shown in Fig. 3. There is considerable scatter within the data however the addition of SiC is seen to cause a decrease in average wear rate, and this decrease is extended when Y_2O_3 sintering aid is added.

For each material type typical eroded surfaces are shown in Fig. 4, and typical fracture surfaces in Fig. 5. Fig. 6 shows the fraction of transgranular fracture measured on the eroded and fractured surfaces. The materials with SiC show a greater tendency towards transgranular fracture after both erosive wear and fracture in 3-point bending.

3.2. Indentation model

Fig. 7 shows a set of indentation grids on a nanocomposite material with Y_2O_3 sintering aid. It can be seen that the grids made at wide spacing (40 and 34.6 μm) tend not to result in damage to the surrounding surface. However as the indentation spacing decreases, damage starts to occur within the grids and results in material being lost from the surface. The severity of the damage continues to increase as the indentation spacing decreases.

Typical height maps derived from optical profilometry are shown in Fig. 8 for widely spaced grids (undamaged) and for more closely spaced grids (damaged). The volume of impression below the surface level varies between 1.2×10^3 μm^3 for the undamaged grid (Fig. 8a) and 1.8×10^4 μm^3 for the severely damaged grid (Fig. 8b). For the undamaged grid this volume represents the volume of the 9 plastic hardness impressions whilst for the damaged grid this volume includes both the volume of material lost from the surface and the plastic hardness impressions. The maximum recorded depth also varies from 3.2 μm for the undamaged grid to 11.9 μm for the severely damaged grid.

In Fig. 8d a grid with moderate damage shows a high point (white) around the central indent which indicates that some lateral cracking has occurred and allowed the surface to lift up. This raised section of material has remained attached to or resting on the underlying material resulting in only 2.5×10^3 μm^3 material having been "lost" from the surface. However when this sample was immersed in ethanol and ultrasonically cleaned for 2 min the raised flake was removed (Fig. 8c), and the volume of material lost increased significantly to 7.2×10^3 μm^3. The effect of ultrasonic cleaning on the volume of material lost from the surface is also illustrated in Fig. 9. In erosive wear testing loose material is likely to be removed by continuing impacts and

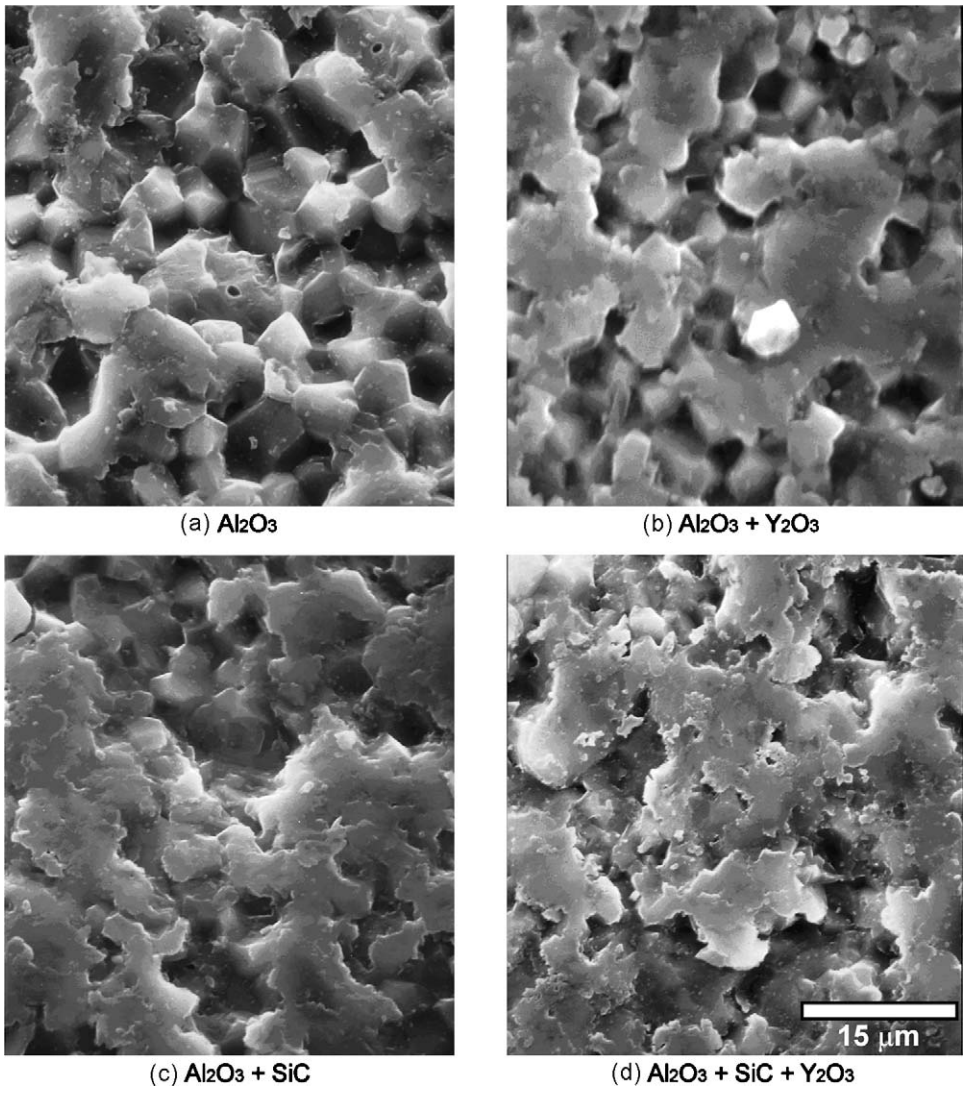

Fig. 4. Surfaces after 12 h erosive wear (all to same scale). Fracture appears to be predominately intergranular except for the materials with SiC added (c and d) which show a greater degree of transgranular fracture.

by the fluid flow. Hence the volume measured after cleaning is expected to be more representative of an erosive wear situation and it is these values that are considered in this paper.

Fig. 10 shows the volume of material lost plotted against grid spacing for all the material types tested. The transition in volume of material lost from a low to a high value occurs at closer grid spacing for materials containing SiC (between 26.0 and 30.0 μm) than for those without (between 30.0 and 34.6 μm). The volume of material lost from severely damaged grids is also reduced for materials containing SiC ($\sim 1.8 \times 10^4$ μm^3) compared to those without SiC ($\sim 2.2 \times 10^4$ μm^3). There is no clear difference between materials with and without Y_2O_3 sintering aid additions.

The differences in fracture mode seen after erosive wear and 3-point bending are also reflected in the lateral cracking that occurs within the indentation grids. Figs. 11 and 12 show nominally undamaged 40 μm spaced grids in Al_2O_3 and a nanocomposite respectively. FIB trenches across both grids reveal sub-surface lateral cracking. Thermal etching reveals that in the Al_2O_3 material the crack follows an intergranular path, while in the nanocomposite material the fracture path is transgranular.

4. Erosive wear rate modelling

Franco and Roberts' model[23] uses the concept that there is a critical distance between impacts from erodent particles below which lateral fracture from each impact links up and results in the loss of material. The critical spacing at which damage from neighbouring impacts links up can be estimated as the spacing at which damage starts to occur within indentation grids, and the volume of material lost with each of these critical impacts can be estimated by the volume measured using optical profilometry.

The critical spacing at which damage starts to occur can be taken as the spacing between indentations when a significant volume of material starts to be lost from the sample. We set this volume as 1×10^4 μm^3 (indicated by the dotted line in Fig. 10) which is mid-way between "high" and "low" values. To define a

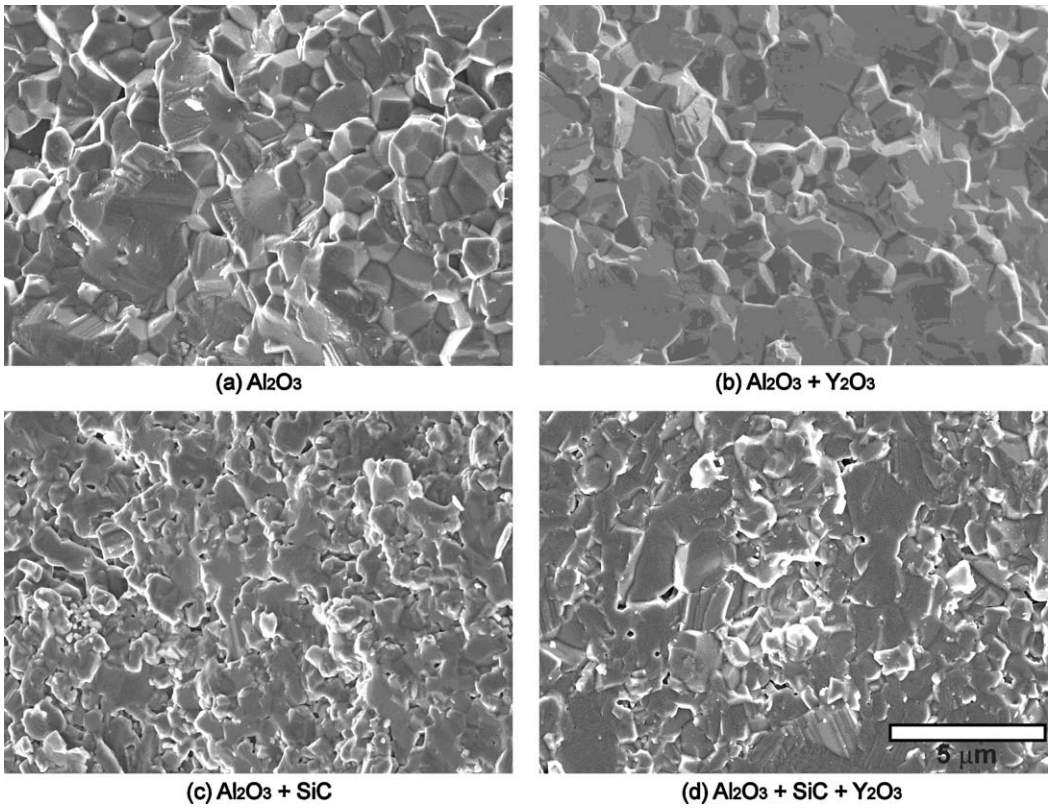

Fig. 5. Fracture surfaces created by 3-point bending (all to same scale).

critical spacing the grid spacing at which this volume is lost from the sample is interpolated between the grids above and below the significant volume. These values are given for each material in Table 2. The area encompassed by this critical radius is taken as the area primed by a single erosion impact.

The average crater volume for grids below the critical spacing is given for each material in Table 2. These volumes represent the

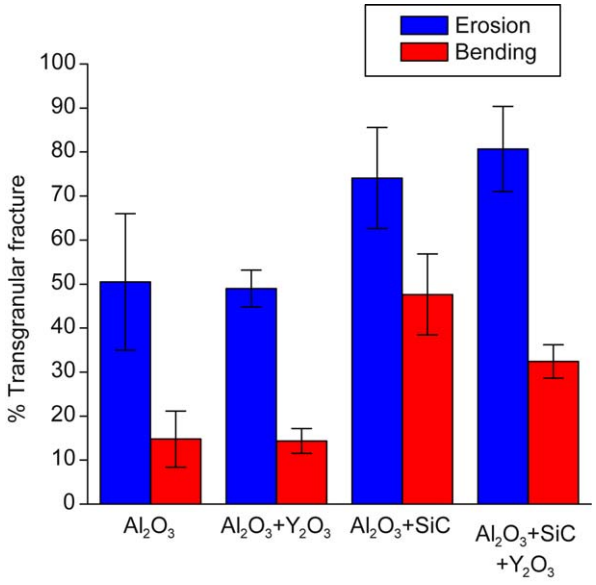

Fig. 6. Percentage of transgranular fracture area on eroded surfaces and fracture surfaces created by 3-point bending.

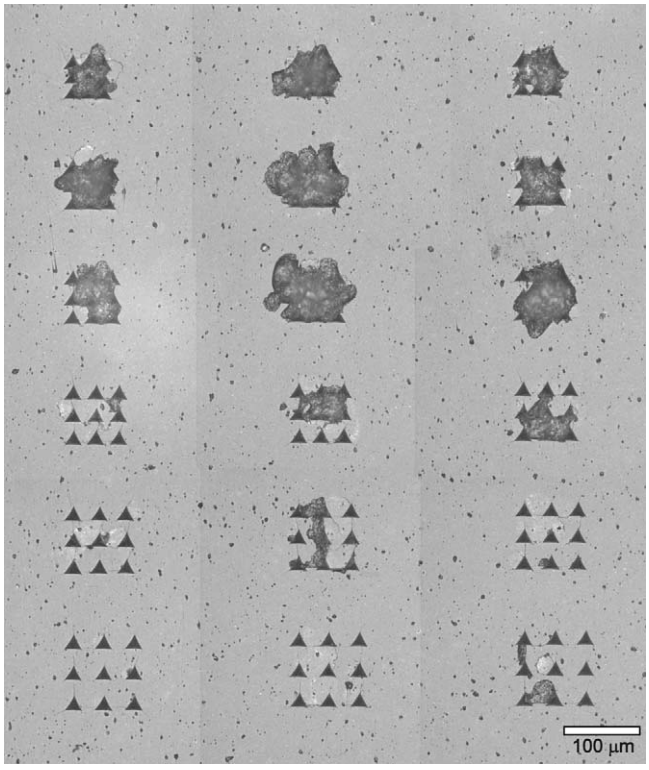

Fig. 7. Optical image of 3 sets of indentation arrays of grids of between 19.6 and 40.0 μm spacing for the nanocomposite material containing Y_2O_3 sintering aid.

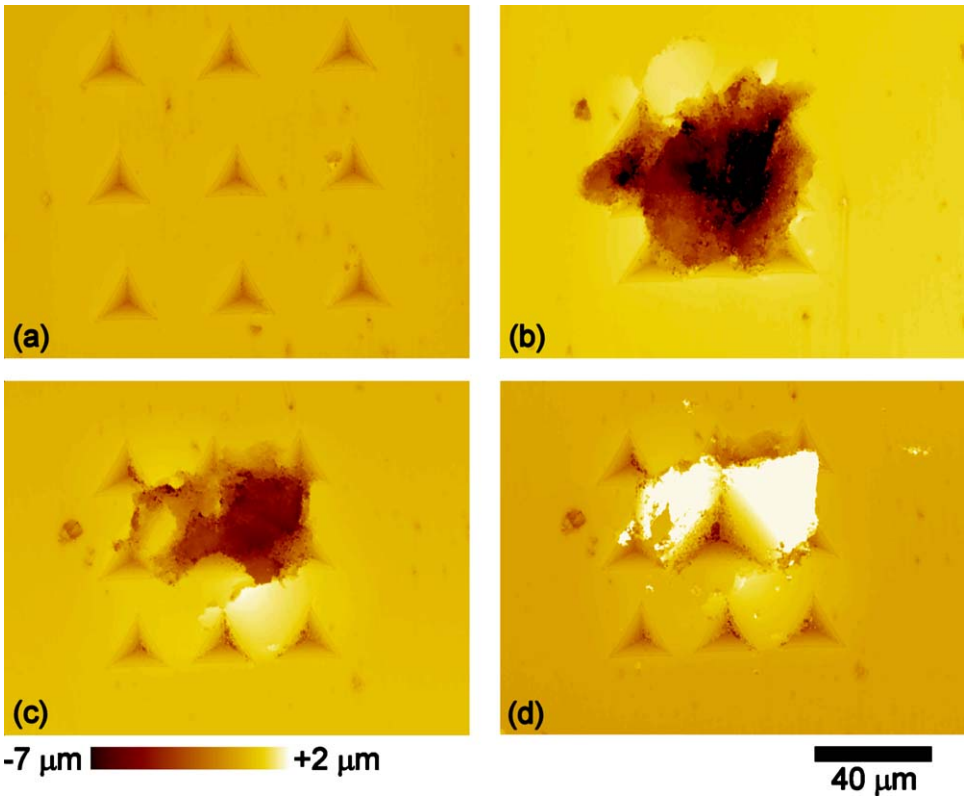

Fig. 8. Optical profilometry height maps of indentation grids in the nanocomposite material containing Y_2O_3 sintering aid. Image (a) is an undamaged 40 μm spaced grid (1.2×10^3 μm^3 impression volume); (b) is a severely damaged 22.5 μm spaced grid (1.8×10^4 μm^3 material lost); (c) and (d) are the same 30 μm spaced grid after cleaning (c, 7.2×10^3 μm^3 material lost) and before cleaning (d, 2.5×10^3 μm^3 material lost).

material lost resulting from 9 sub-critically spaced indentations, i.e. a grid which has 12 nearest neighbour spacings. The volume of material lost due to a pair of critically spaced erodent impacts is estimated as one-twelfth of the average crater volume from each sub-critically spaced grid.

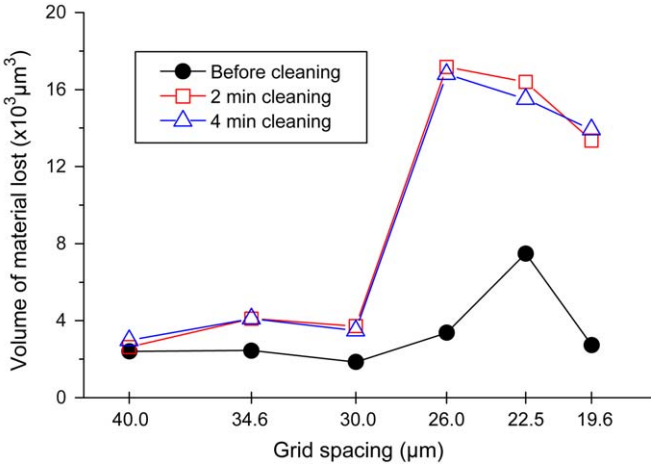

Fig. 9. The volume of material lost from the surface of the nanocomposite sample as a result of indentation grids at various spacings averaged over 3 repeats at each spacing. The circular points show the volume before cleaning whilst the squares show the volume lost after ultrasonic cleaning for 2 min. The triangles are repeated optical profilometry measurements of the same grids after a further 2 min ultrasonic cleaning.

Franco and Robert's model also includes a term for the area of surface that is removed in each chip (and is therefore no longer primed). The area of the crater was not conveniently measured using optical profilometry; however an estimate could be made using the depth of the craters (given in Table 2). If the depth to area ratio of the crater is assumed to be 1:3 (e.g. a quarter of a sphere) the worn area is 3 times the crater volume divided by the maximum depth.

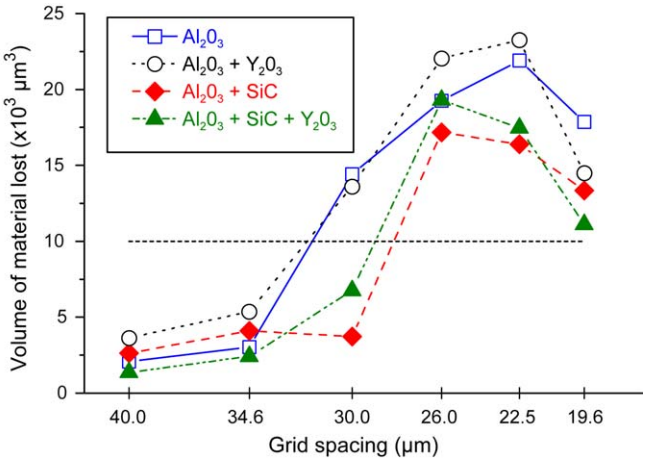

Fig. 10. The volume of material lost against grid spacing plotted for all four materials studied. The volume lost is generally reduced for the materials containing SiC. The dashed horizontal line is proposed as an arbitrary transition above which material starts to be 'eroded' from the surface.

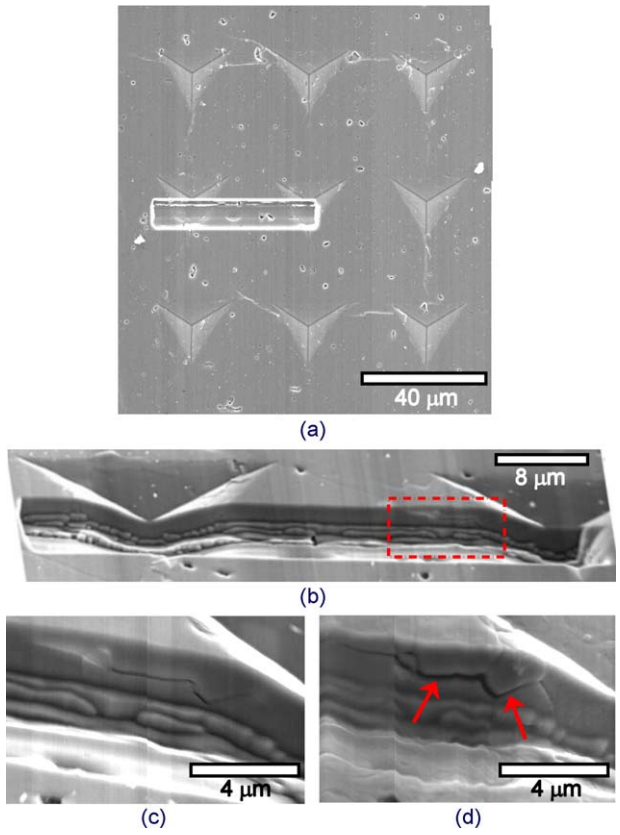

Fig. 11. SEM images of a stepped trench in a 40 μm grid in pure Al_2O_3 shown flat in (a) and at 60° tilt in (b) to show the 'polished' section. The area in the dotted box is detailed unetched in (c) and thermally etched in (d). Intergranular cracking is indicted by arrows.

The estimates for area primed, the volume of material lost due to a pair of critical impacts, the surface area removed and the flux of particles ($8.60 \times 10^7\ m^{-2}\ s^{-1}$) previously measured for the erosive wear tester used in this work[14] are used as inputs for the model (Eq. (4)) to estimate erosive wear rates. These are given in Table 2, and compared with the experimental values. Though the trends in experimental erosive wear rate are reproduced by the model, the modelled values are ~10× higher than the experimental ones. This is discussed in the following section.

5. Discussion

5.1. Wear and fracture behaviour

The variations in erosive wear rate of the materials studied here are consistent with previous results for Al_2O_3 and Al_2O_3–SiC nanocomposites.[8–11,15–17] The erosive wear rate is reduced when SiC is added either with or without the sintering aid addition. Wear rate in Al_2O_3 is always dependent on grain size[13] so some caution has to be exercised to ensure that the improvement in wear rate is not simply because of grain size refinement (Table 1) due to grain boundary pinning by SiC.[25] However when grain size is carefully controlled most researchers consider that the SiC addition improves the wear resistance of Al_2O_3.[3,8,10,20] The reduction in wear rate when Y_2O_3 sintering aid was added to the nanocomposite material is certainly significant as there is a slight increase in grain size when this addition is made.

The change in fracture mode from intergranular to transgranular when SiC is added is clear and consistent with previous data.[5,6] Fracture paths in 3-point bending fracture surfaces, erosive wear surfaces and sub-surface cracks within indentation grids all show this transition.

5.2. Indentation model of erosive wear

The difference in response of the materials to indentation was clear from visual inspection of the indentation grids. The Al_2O_3/SiC material resisted chipping between indentations to closer spacings compared to plain Al_2O_3. The profilometry values for volume of material lost confirmed this trend. The increase in volume lost occurred at wider grid spacings for Al_2O_3 compared to the nanocomposite. The nanocomposite materials also showed reduced crater volume once damage did occur. However, no obvious effect of Y_2O_3 addition was seen either with or without SiC (Fig. 10).

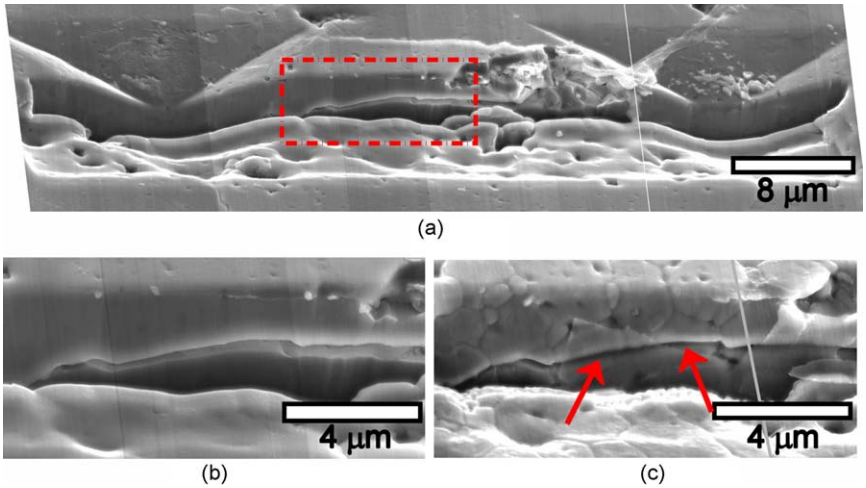

Fig. 12. SEM images of the 'polished' section of a stepped trench in a 40 μm grid in Al_2O_3 with SiC added (a). The area in the dotted box is detailed unetched in (b) and thermally etched in (c). Transgranular cracking is indicated by arrows.

Table 2
Experimental values for critical grid spacing, average volume lost from grids and crater depth plus calculated values for primed area (a_p), worn area (a_w) and modelled erosive wear rate (R). Experimental erosive wear rates at a lower impact load are included for comparison.

Material	Critical grid spacing (μm)	Primed area, a_p ($\times 10^{-10}$ m^2)	Average volume lost from grid ($\times 10^4$ μm^3)	Crater depth, d (μm)	Worn area, a_w ($\times 10^{-10}$ m^2)	Modelled wear rate, R (4.9 N indents) (nm s^{-1})	Experimental wear rate (2 N impacts) (nm s^{-1})
Al_2O_3	31.8	7.93	1.84	11.45	4.01	87	9.2
$Al_2O_3 + Y_2O_3$	32.0	8.05	1.83	10.27	4.47	85	8.2
Al_2O_3 + SiC	28.1	6.22	1.56	9.20	4.25	67	6.1
Al_2O_3 + SiC + Y_2O_3	29.0	6.59	1.60	9.05	4.41	69	4.1

When the parameters from the indentation grids are used as inputs to Franco and Roberts' model[22] to estimate wear rates, a reduced wear rate is predicted for materials containing SiC (~68 nm s^{-1} compared to ~86 nm s^{-1} for plain Al_2O_3), though no significant effect is predicted for the Y_2O_3 addition. These values are an order of magnitude higher than the experimental erosive wear values (~4 to ~9 nm s^{-1}) and also show a slightly smaller relative difference between Al_2O_3 and nanocomposites. The factors expected to influence the parameters in Franco and Roberts' model and consequently the wear rates predicted by Eq. (4) are discussed below.

5.2.1. Indentation/impact load

Changes in indentation/impact load will influence both the extent and the depth of cracks formed. For an isolated indentation the extent of cracking will depend on the indentation load chosen as well as the materials parameters of hardness, modulus and toughness, with the length of cracks scaling as the 2/3 power of load.[19] Consequently the area primed (a_p) will be expected to scale with the 4/3 power of load. The worn area (a_w) is also related to the extent of cracking from two indentations/impacts so will also be expected to scale with the 4/3 power of load.

The depth at which lateral cracks form is likely to be related to the indentation depth. By definition, hardness is the ratio of load to projected indentation area, hence for a given indent geometry, depth is proportional to the square root of load and the depth (d) of craters is expected to vary similarly.

If these relationships are all considered Eq. (4) is expected to show that predicted wear rate (R) will depend on load to the power 11/6. In the present work indentations were made at ~2.5 times the load that Franco and Roberts[14] measured for the erodent particles impacts in the erosive wear equipment. Hence the wear rates predicted are expected to overestimate the experimental values by ~5.4 times. (Indentations were not made at a lower load as this would have required more closely spaced grids which would be more sensitive to surface imperfections, and because the reduced volume of material lost would also have been more difficult to measure accurately.)

A further effect may be that the lower effective loads for impacts encountered in the wear test may not always initiate a fracture event. The inhibition of crack initiation in the nanocomposites[7] would then produce an additional reduction in wear rate compared to alumina. The rate of loading will also be different between indentation and erosion which may result in different fracture behaviour.[26]

5.2.2. Criterion for primed area

The critical spacing from the indentation grids was determined using a fairly arbitrary criterion for the volume threshold which was considered to be 'significant' damage. This threshold was used to define the area primed (a_p) hence the criterion selected will alter the predicted wear rate.

5.2.3. Criterion for volume lost

The indentation model also involved grids of 9 indentations, rather than pairs of impacts as considered in Franco and Roberts' model.[22] The grid of 9 indentations has 12 nearest neighbour gaps so the volume of material lost from the grids was taken to represent 12 times that which would have been lost due to a pair of impacts. This assumption allows the worn area (a_w) to be calculated using the volume, depth and shape of the crater. However if the volume lost was not due to 12 nearest neighbour interactions an error will be introduced into the predicted wear rate.

5.2.4. Shape of wear craters

An assumption for the shape of wear craters (shape factor, α) was necessary to calculate the worn area (a_w) using the volume and depth (d) of the craters within indentation grids and hence if false this assumption will alter the predicted wear rate. If the shape of craters is similar between materials this will represent a systematic error; however if different fracture paths in different materials lead to different shaped craters the relative values may be affected. For example, if the transgranular fracture mode in nanocomposites creates a shallower crater, the predicted wear rate will be exaggerated for nanocomposites.

5.2.5. Measurement errors

All the inputs are subject to measurement errors. For example, an error in the flux of erodent particles[14] would also cause a discrepancy between experimental and predicted wear rates. These errors however would not be expected to influence the trends between materials.

Despite these sources of uncertainty the model (outlined in section 1.3) is thought to reflect the fracture process that occur during erosive wear and the fit to a factor of ~2 between the observed and (load-corrected) predicted erosive wear rates indicates that the model is valid.

5.3. Mechanism for erosive wear

The mechanism for erosive wear described by the indentation model together with the change in fracture path between Al_2O_3 and nanocomposites suggest that the erosive wear rate difference between the two materials is controlled by changes in fracture behaviour. A reduction in extent of lateral cracking around impacts or indentations reduces the primed area and hence wear rate. A reduction in primed area was observed for grids in nanocomposites compared to Al_2O_3. Similarly the volume of material removed once damage does link up was also reduced for nanocomposites compared to Al_2O_3 which will also result in reduced erosive wear rate.

As has previously been suggested for abrasive wear of Al_2O_3 and Al_2O_3–SiC nanocomposites,[7] changes in the path of lateral cracks can reduce the volume of material chipped away from the surface. A transgranular fracture path could allow a fraction of a grain to be removed as a chip where as intergranular fracture may force the crack to propagate around a whole grain. The change in fracture mode to transgranular for nanocomposites during erosion could be considered to reduce both the primed area and the volume of material lost due to impacts of erosive particles. This change in fracture path between Al_2O_3 and nanocomposites was directly observed for shallow lateral cracks (Figs. 11 and 12) although the depth of indentation craters measured suggest that deeper lateral cracks would also be involved for erosive wear at similar impact loads.

6. Conclusions

Erosive wear testing has shown a reduction in wear rate for Al_2O_3–SiC nanocomposite materials compared to Al_2O_3. Consistent with previous work, this change is attributed to a genuine change in erosive wear behaviour due to the presence of SiC, as the variations in grain size between the different materials tested were minor. A clear change in fracture mode with the addition of SiC was also observed on wear and fracture surfaces and around indentations, consistent with previous studies.

Grids of indentations have been used to model the effect of particle impacts on a ceramic surface during erosion. This model has been shown to be effective in distinguishing, both qualitatively and quantitatively, between Al_2O_3 and Al_2O_3–SiC nanocomposite materials. Experimental constraints limited the similarity of particle impact/indentation load in the direct erosion experiments and the indentation-grid model; however, the wear rates predicted (67–87 nm s^{-1}) by the indentation model, when adjusted for the likely effects of these differences in load (giving ~12 to ~16 nm s^{-1}) are in reasonable agreement with those measured directly in erosive wear tests at lower impact load (4–9 nm s^{-1}). It should be noted that whilst some assumptions were necessary to calculate a predicted wear rate using the indentation model no fitting or calibration parameters were used. This supports the validity of the mechanism proposed by Franco and Roberts[22] for material removal during low-speed impact erosive wear of ceramics, in which sub-surface cracking generated by a particle impact is needed before subsequent impacts cause damage to link up and material to be lost.

This work also implies that the differences in erosive wear rate between Al_2O_3 and Al_2O_3–SiC nanocomposites can be linked to the change from intergranular fracture in Al_2O_3 to trangranular fracture in Al_2O_3–SiC nanocomposites, as has been previously described for abrasive wear of similar materials.[7]

Acknowledgements

This research was supported by the Engineering and Physical Sciences Research Council (UK), under grant N06601.

References

1. Niihara K, Nakahira A. Strengthening and toughening mechanisms in nanocomposite ceramics. *Ann Chim France* 1991;**16**(4–6):479–86.
2. Niihara K, Nakahira A. Particle strengthened oxide nano-composites. In: Vincenzini Q, editor. *Advanced structural inorganic composites*. Elsevier Science Publishers; 1991. p. 637.
3. Davidge RW, Brook RJ, Cambier F, Poorteman M, Leriche A, O'Sullivan D, Hampshire S, Kennedy T. Fabrication, properties and modelling of engineering ceramics reinforced with nanoparticles of silicon carbide. *Br Ceram Trans* 1997;**96**(3):121–7.
4. Carroll L, Sternitzke M, Derby B. Silicon carbide particle size effects in alumina-based nanocomposites. *Acta Mater* 1996;**44**(11):4543–52.
5. Zhao J, Stearns LC, Harmer MP, Chan HM, Miller GA. Mechanical behaviour of alumina-silicon carbide "nanocomposites". *J Am Ceram Soc* 1993;**76**(2):503–10.
6. Borsa CE, Jiao S, Todd RI, Brook RJ. Processing and properties of Al_2O_3/SiC nanocomposites. *J Microsc* 1995;**177**(3):305–12.
7. Limpichaipanit A, Todd RI. The relationship between microstructure, fracture and abrasive wear in Al_2O_3/SiC nanocomposites and microcomposites containing 5 and 10% SiC. *J Eur Ceram Soc* 2009;**29**(13):2841–8.
8. Ortiz-Merino JL, Todd RI. Relationship between wear rate, surface pull-out and microstructure during abrasive wear of alumina and alumina/SiC nanocomposites. *Acta Mater* 2005;**53**(12):3345–57.
9. Walker CN, Borsa CE, Todd RI, Davidge RW, Brook RJ. Fabrication, characterisation and properties of alumina matrix nanocomposites. *Br Ceram Proc* 1994;**53**:249–64.
10. Kara H, Roberts SG. Wet erosion behaviour of low SiC alumina–SiC nanocomposites. *J Mater Sci* 2002;**37**(12):2421–6.
11. Kara H, Roberts SG. Polishing behaviour and surface quality of alumina and alumina/silicon carbide nanocomposites. *J Am Ceram Soc* 2000;**83**(5):1219–25.
12. Hutchings IM. Ductile-brittle transitions and wear maps for the erosion and abrasion of brittle materials. *J Phys D: Appl Phys* 1992;**25**(1A):A212–21.
13. Miranda-Martinez M, Davidge RW, Riley FL. Grain size effects on the wet erosive wear of high-purity polycrystralline alumina. *Wear* 1994;**172**(1):41–8.
14. Franco A, Roberts SG. Controlled wet erosive wear of polycrystalline alumina. *J Eur Ceram Soc* 1996;**16**(12):1365–75.
15. Kumar CS, Baron B, Hampshire S. Effect of Y_2O_3 on pressureless-sintering and erosive wear resistance of Al_2O_3–5 vol.% SiC nanocomposite. *Br Ceram Proc* 1999;**60**:395–6.
16. Bajwa S, Rainforth WM, Lee WE. Sliding wear behaviour of SiC–Al_2O_3 nanocomposites. *Wear* 2005;**259**(1–6):553–61.
17. Guicciardi S, Sciti D, Melandri C, Bellosi A. Dry sliding wear behavior of Al_2O_3–SiC submicro- and nano-composites. *J Am Ceram Soc* 2005;**88**(1):179–83.
18. Evans AG, Wilshaw TR. Quasi-static solid particle damage in brittle solids—I. Observations, analysis and implications. *Acta Metall* 1976;**24**(10):939–56.
19. Anstis GR, Chantikul P, Lawn BR, Marshall DB. A critical evaluation of indentation techniques for measuring fracture toughness. *J Am Ceram Soc* 1981;**64**(9):533–8.

20. Sedláček J, Galusek D, Švančárek P, Riedel R, Atkinson A, Wang X. Abrasive wear of Al_2O_3–SiC and Al_2O_3–(SiC)–C composites with micrometer- and submicrometer-sized alumina matrix grains. *J Eur Ceram Soc* 2008;**28**(15):2983–93.
21. Franco A, Roberts SG. The effect of impact angle on the erosion rate of polycrystalline α-Al_2O_3. *J Eur Ceram Soc* 1998;**18**(3):269–74.
22. Franco A, Roberts SG. Wet erosive wear of alumina. In: *Paper presented at 'international conference on erosive and abrasive wear'*. 1998.
23. Franco A, Roberts SG. The use of closely spaced vickers indentations to model erosion of polycrystalline alpha-Al_2O_3. In: Basu SN, Krzanowski JE, Patscheider J, Gogotsi Y, editors. *Materials research society symposium proceedings, vol. 843*. 2005. p. 143.
24. Twigg PC, Davidge RW, Riley FL, Franco A, Roberts SG. Indentation-induced crack interaction in alumina ceramics. *Philos Mag A* 1996;**74**(5):1245–52.
25. Shapiro IP, Todd RI, Titchmarsh JM, Roberts SG. Effects of Y_2O_3 additives and powder purity on the densification and grain boundary composition of Al_2O_3/SiC nanocomposites. *J Eur Ceram Soc* 2009;**29**(9):1613–24.
26. Rowcliffe DJ. Quasi-static indentation of ceramics. *Key Eng Mater* 1992;**71**:1–22.